# A GPR Able to Detect Its Own Position Using Fixed Corner Reflectors on Surface

# A GPR able to detect its own position using fixed corner reflectors on surface

Lapo Miccinesi, Member, IEEE, and Massimiliano Pieraccini, Member, IEEE

**Abstract — Ground penetrating radar (GPR) systems are equipment able to acquire underground images scanning the surface of the soil/pavement under investigation. Usually GPR records its own position along the scan line using a mechanical odometer, i.e. a rolling wheel in contact with the ground. Unfortunately, this simple and cheap solution can be not effective on uneven terrains. In this paper a completely different solution is proposed for retrieving the radar position along the scan. An additional couple of transmitting/receiving (TX/RX) antennas detects the distance of one or two corner reflectors (CR). As the signal backscattered by the CR appears in GPR trace (with a suitable delay for separating air and ground signals) the position data are co-registered in the radar trace itself and no external synchronization is necessary. The technique has been successfully tested both for detecting the position of the radar along a line (one-dimensional case), and on a surface (two-dimensional case).**

**Index Terms — ground penetrating radar, interferometry, odometer, positioning, radar.**

## I. Introduction

GROUND penetrating radar (GPR) systems are widely used for investigating the ground up to 2-3 m deep [1,2]. Typically, a GPR scans a surface and records its own position along the scan line using a mechanical odometer, i.e. a rolling wheel in contact with the ground. This is a simple and effective solution for asphalted or paved surfaces. Due to the popularity of Global Positioning System (GPS) devices, most of today's GPR instruments are able to interface with standard GPS devices [3] or they are provided with an integrated GPS receiver [4]. As a result, data loggers combine the GPR and the GPS data during acquisition. This is a common practice for geological surveys [5] and in archeological prospections [6]. The main limitation of GPS is its poor accuracy (5-6 m) [7]. Differential GPS can be a solution, but its cost can be prohibitive in many GPR applications. Nevertheless, any GPS device has serious problems of coverage in many areas and in closed spaces. Therefore, alternative solutions have been proposed. A GPS can be integrated with an inertial measurement unit (IMU), but the fusion between IMU e GPS data is not trivial because of drifts, delays, and measurement errors [7,8,9]. Indeed, IMU is often used just for detecting the orientation of the antennas [7]. A laser theodolite tracking the GPR is another possible solution that has been tested [10]. A rotary laser system miming the GPS in small scale has been also proposed as positioning system for a GPR operating in rough terrains [3]. Other researchers developed positioning systems based on cameras [11,12,13].

All these methods require additional equipment that has to be synchronized with the radar acquisition. This task can be rather complex using off-the-shelf radar, due to possible problems with uncontrolled delays or jitter.

The solution we propose in this paper is completely different from previous ones. A GPR is modified in order to have an additional couple of transmitting/receiving (TX/RX) antennas in front of the GPR. The radar transmits and receives at the same time to/from both the couples of antennas. So, the radargram contains two mixed signals: the underground signal and the air signal. A RF cable introduces a suitable delay in the signal in air in order to clearly separate in time the two signals. One or two corner reflectors (CR) are located in fixed positions in the field of view (in air) of the radar. The signal backscattered by the CR is used for detecting the position of the GPR during the scan. The major advantages of this technique are two: 1) it does not require a specific device for positioning, but just a second couple of antennas; 2) the position data are co-registered in the radar trace, so no external synchronization is necessary.

## II. Working Principle

Fig. 1 shows a sketch of the GPR modified with an additional couple of TX/RX antennas operating in air and positioned in front of the radar equipment.

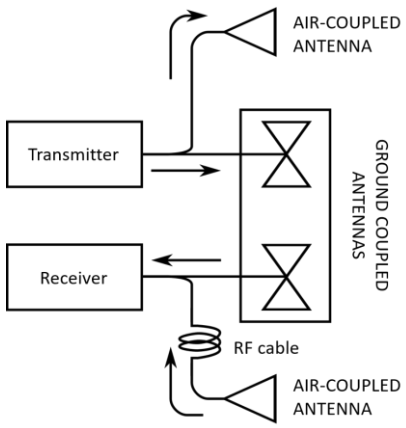


Fig. 1. Sketch of the modified GPR system.

The Authors are with the Department of Information Engineering, University of Florence, via Santa Marta 3, 50129 Firenze, Italy (e-mail: lapo.miccinesi@unifi.it).

As the radargram contains two mixed signals (the underground and the air signals) an RF cable is connected to the one of the air-coupled antennas for introducing a suitable delay that separates the two contributes.

Generally speaking, the position of the GPR can be retrieved using the signal of one or more CR in the field of view of the additional (air-coupled) antennas of GPR. Nevertheless, the odometer (that measures the traveled path) can be suitably replaced by a single CR located in front of the radar.

In order to test the working principle of the proposed technique, a simulation has been carried out. With reference to Fig. 2, a fixed CR is positioned in front of the radar. An underground target is located 5 m in front of the radar, 0.5 m below the ground surface. The dielectric constant of ground is supposed 9.0 and the attenuation 10dB/m. The GPR moves 10 m along x-direction from its initial position (12 m far from the CR).

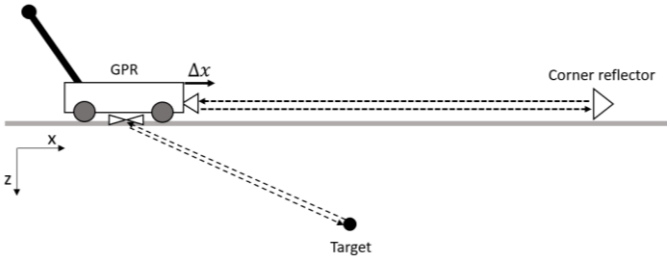


Fig. 2. Working principle of the modified GPR system.

The GPR transmits a continuous wave step frequency (CWSF) signal sweeping from 100 MHz to 1 GHz with 201 frequencies. The radar is supposed to move slowly with respect to the frequency sweep time, so the radar can be considered not moving during each single sweep. The air-equivalent length of RF cable is 7.5 m. Finally, Gaussian noise is added to the simulated echo (signal-to-noise ratio: 20 dB). Fig. 3 shows the result of the simulation. The radargram has been obtained as Inverse Fast Fourier Transform (IFFT) of the simulated echo in frequency domain to which a Hann-window had been applied.

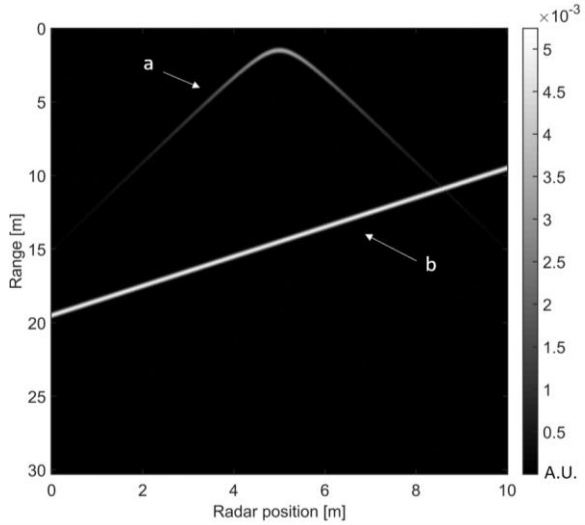


Fig. 3. Simulated radargram of modified GPR.

The hyperbola marked with **a** is related to the underground target. The signal marked with **b** is related to the CR. The two contributes are well-separated in range.

The position of the CR peak gives a rough estimate of the radar-CR distance. Indeed, its accuracy is comparable with the range resolution: c/2B (where c is the speed of light and B is the bandwidth). In this simulation the range resolution is about 0.15 m. This accuracy is not enough to retrieve the radar position better than with odometer.

Another way for retrieving the GPR position along the scan line is to use the phase information of the CR. Indeed, the displacement of the radar, Δx, is related to difference of phase, Δϕ,between two successive acquisitions:

$$\Delta x = \frac{c}{4\pi f_0}\Delta\phi \qquad (1)$$

where $f_0$ is the frequency of the radar signal. This interferometric approach can give accuracy much higher than peak detection. An important question related to eq. (1) is the value of frequency $f_0$ to use. If the frequency response of the radar system with its antennas is a symmetric function (for example a rect or a Guassian) $f_0$ is the central frequency. But this is not the case for the air-coupled horn antennas used in this prototype. Indeed, they have a cut-off frequency at about 0.5 GHz and a low-frequency slope of 80 dB/GHz as shown in Fig.4. Using this frequency response, the central frequency has to be multiplied by 1.28.

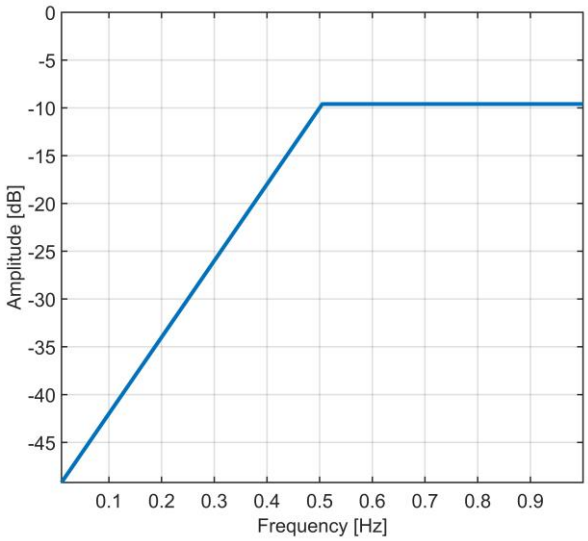


Fig. 4. Frequency response of the couple of air-coupled horn antennas used in simulation.

Usually the interferometric approach is used for detecting the movement of targets that do not change their range-bin. But, as shows in Fig. 3, the range-bin of CR changes with x. For this reason, a range sliding-window has been used as shown in Fig. 5.

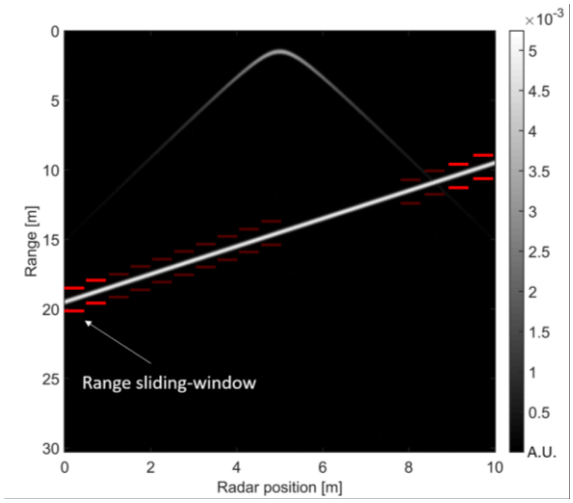


Fig. 5. Simulated radargram of modified GPR with example of range sliding-window for searching the corner reflector peak.

The initial window, 2 m wide, is centered around the first position of CR. The peak of corner reflector is searched inside this window. The peak position is the center of the subsequent window. The phase difference between $(i+1)^{th}$ and $i^{th}$ measurements is calculated at the range value of the center of $i^{th}$ window as shown in Fig. 6

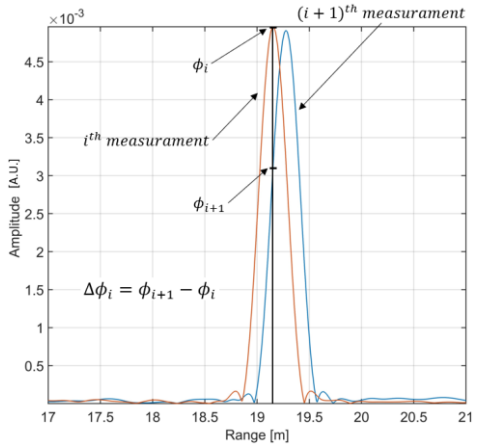


Fig. 6. Example of phase measurement for detecting the GPR position.

The GPR displacement is evaluated using the (1). The integrated result is shown in Fig. 7. The standard deviation of the difference between measured and nominal position resulted 0.47 mm (with simulated data affected by a SNR = 20dB).

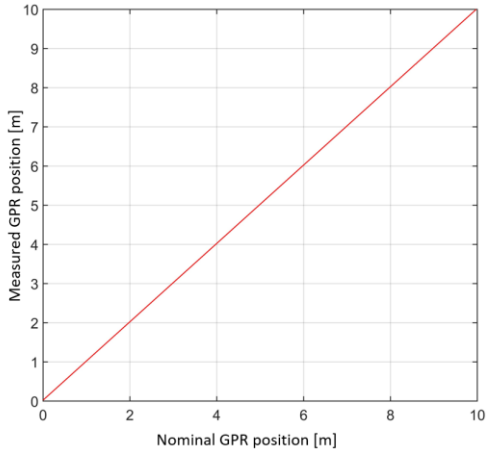


Fig. 7. GPR position evaluated with (1).

The same approach can be extended to the two-dimensional case. i.e. for tracking the GPR on the horizontal plane. In this case, two CR are necessary. The CR are located in the field of view of the air-coupled antennas as shown in Fig. 8.

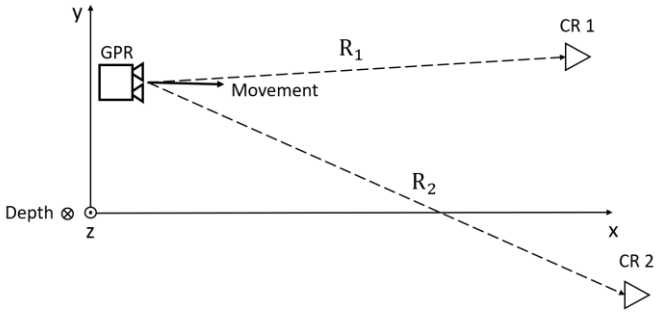


Fig. 8. GPR positioning using two CR.

For using this technique, the positions of the CR and the initial position of GPR have to be known. With reference to Fig. 8 the GPR is able to measure the k-th distance $R_{1,k}$ and $R_{2,k}$ by the phase difference as follows:

$$R_{1,k} = R_{1,0} + \frac{c}{4\pi f_0}\sum_{i=0}^{i=k}\Delta\phi_{1,i} \quad (2)$$

$$R_{2,k} = R_{2,0} + \frac{c}{4\pi f_0}\sum_{i=0}^{i=k}\Delta\phi_{2,i} \quad (3)$$

where $R_{1,0}$ and $R_{2,0}$ are given by the initial position, $\Delta\phi_{1,i}$ and $\Delta\phi_{2,i}$ are the phase differences relative to CR1 and CR2 measured as described in Fig. 6. The position of GPR can be evaluated solving the system:

$$\begin{cases} R_{1,k}^2 = (x_1 - x_{R,k})^2 + (y_1 - y_{R,k})^2 \\ R_{1,k}^2 = (x_2 - x_{R,k})^2 + (y_2 - y_{R,k})^2 \end{cases} \quad (4)$$

where $(x_1,y_1)$ is the position of CR1, $(x_2,y_2)$ is the position of CR2, $(x_{R,k}, y_{R,k})$ is the k-th position of the radar.

For each k-th position, the system has two solutions as shown in Fig. 9. One of the two trajectories is not physical and has to be discharged.

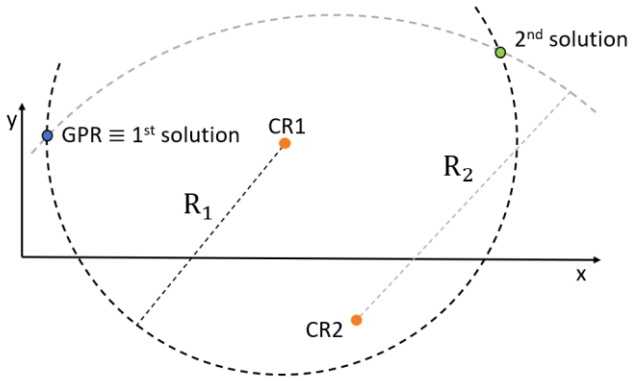


Fig. 9. Example of solution of system (4).

By supposing CR1 located in $(12\ \mathrm{m}, 0\ \mathrm{m})$ and CR2 in $(14.5\ \mathrm{m}, 2.5\ \mathrm{m})$, a simulation has been carried out using the same GPR parameters as before. Fig. 10 shows the retrieved two trajectories: the blue line is the GPR trajectory, the green line is the (not physical) second solution.

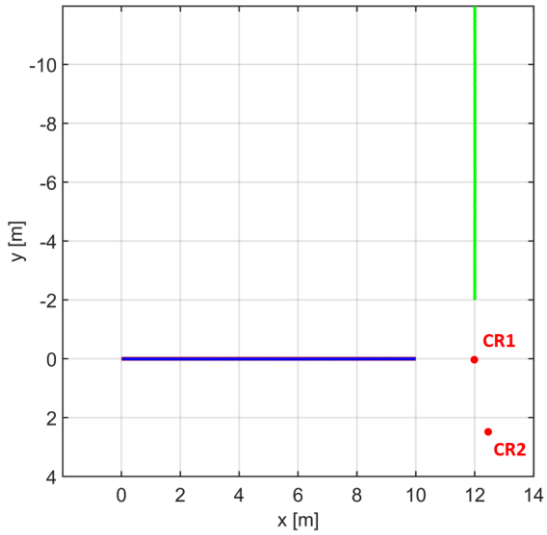


Fig. 10. Example of retrieved position of GPR using (4). The blue line is the GPR position, the green line the 2nd solution

Generally speaking, radar interferometry is able to detect a displacement provided that inside the resolution bin there is only a single target, therefore the method cannot work when the radar traces of CR1 and CR2 are closer than the resolution. In the practice the method fails when

$$|R_1 - R_2| < \alpha \frac{c}{2B} \tag{5}$$

where α is a coefficient that depends on windowing applied before IFFT. Furthermore, as above mentioned, for each position of GPR, the system in eq. (4) gives two solutions of which only one is physical, and these two solutions result coincident when the radar is in the straight line that connects CR1 e CR2.

In order to illustrate these concepts, Fig. 11 shows a simulation where the radar travels horizontal lines from left to right (the CR are positioned as before mentioned). The blue lines are the paths retrieved from the first solution of the system in eq. (4).

The red lines are the effective paths. The blue lines perfectly overlap the red lines in the zone at right of the thick orange line (the straight line that connects CR1 and CR2) and at the edge of the gray zone. This zone has been calculated as locus where $|R_1 - R_2| > \beta \frac{c}{2B}$ with β=2. This is consistent with the fact that the method fails when the radar traces of CR1 and CR2 are too close. Furthermore, it is interesting to note that along the orange line the two solutions of the system in eq. (4) swap: at the left of the orange line the physical solution is the first one, while at the right of the orange line the physical solution is the second one.

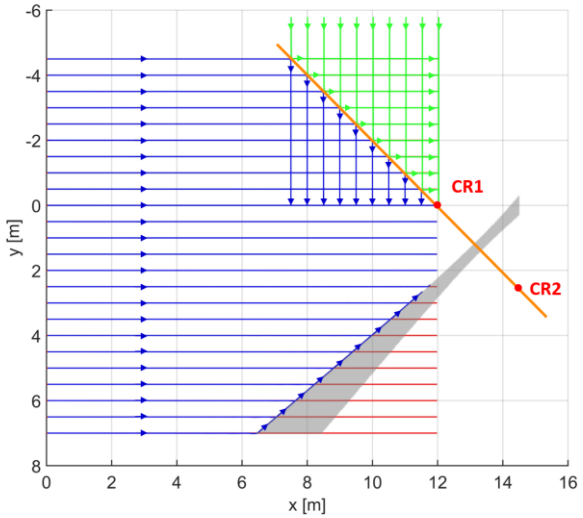


Fig. 11. Map of the radar paths retrieved with the method of the two CR

On the basis of Fig.11, we can state that, as rule of thumb, the method of the two CR is effective in the zone limited by the straight light connecting the two corners and (approximately) the straight light orthogonal to the previous line crossing the median point between the two CR

## III. The Radar Equipment

A block scheme of the modified GPR is shown in Fig. 12. The modified GPR was based on a CWSF prototype, named ORFEUS, developed in the frame of a European Project [14], [15], [16]. ORFEUS sweeps 201 frequencies from 100 MHz to 1 GHz. The transmitting power is 0 dBm and the receiving dynamic range is 100 dB. The unambiguous range of ORFEUS is 30 m in air.

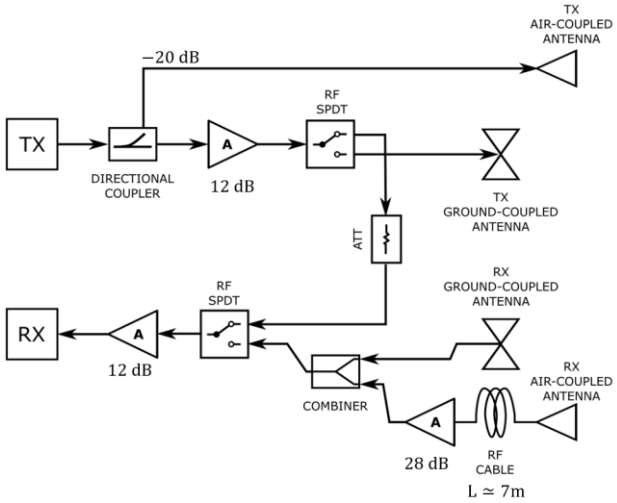


Fig. 12. Block scheme of GPR with additional antennas.

In standard modality the signal coming from the transmitter (TX) is amplified in order to reach 0 dBm at ground-coupled antenna. A couple of Single Pole Double Throw (SPDT) switchers provides a calibration path. The ORFEUS radar has been modified with a directional coupler before the TX-amplifier. Most of the signal goes to the ground transmitting chain, while $-20$ dB is transmitted by the air-coupled antenna. Furthermore, the two received signals are summed using a combiner. An RF cable (air equivalent length: 6.78 m) is connected to the air-coupled receiving antenna for separating the air signal from the ground signal. A 28 dB amplifier increases the air-signal level. This amplifier avoids also a possible double bounce of the ground signal in the air chain.

The air-coupled antennas are double-ridged horn produced by Schwarzbeck Mess, model BBH99120A nominally operating between 800 MHz and 5.2 GHz. The ground-coupled antennas are bow-tie produced by IDS-Georadar with central frequency and bandwidth equal to 200 MHz.

Fig. 13 shows the modified front-end. The transmitter is connected to the TX amplifier through the directional coupler. The couple of SPDT switchers provides the calibration path. The RF cable (blue) introduces the suitable delay for separating the two contributes. The two signals are summed by the combiner and the result is sent to the RX through an amplifier.

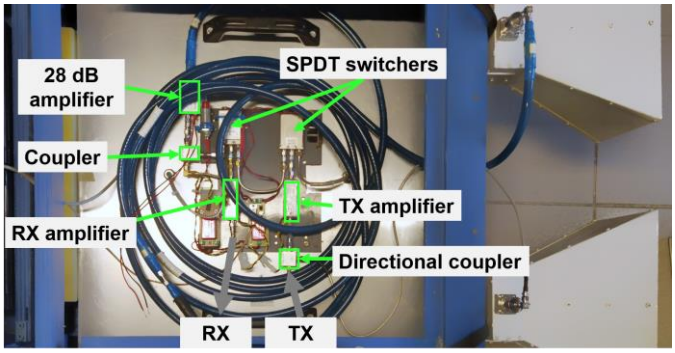


Fig. 13. Modified ORFEUS' front-end.

Usually the signal acquired by a GPR is co-registered with an odometer wheel. In order to do not change the acquisition/co-registration system, an electric motor with a speed-reducer was connected to the axis of odometer, as shown in Fig. 14. This solution can be used for any commercial GPR. The rotation speed of the DC-motor has to be equal or higher than the speed of wheel-odometer during a typical standard measurement. In the experimental test reported in the next chapter the speed has been fixed at 9.38 rpm.

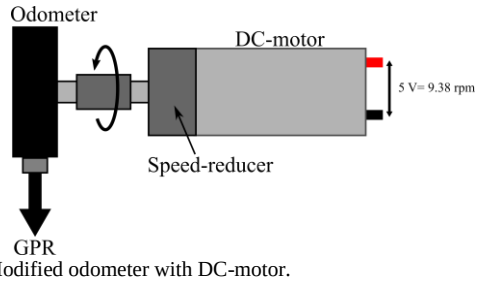


Fig. 14. Modified odometer with DC-motor.

## IV. Experimental Tests

The prototype used for the experimental tests is shows in Fig. 15. It is possible to note the modified odometer over the GPR and the additional couple of antennas in front of the equipment.

Fig. 15. ORFEUS modified with the additional antennas.

This GPR can be used on uneven ground without odometer, but for evaluating the performances of the proposed method some scans have been performed on the asphalt using the odometer wheel.

Fig. 16 shows a picture of the test site. A single metallic CR (side length: 1.4 m) was used as target.

Fig. 16. Test site for evaluating the performances of the modified GPR.

Fig. 17 shows an example of radargram. A background removal was applied after IFFT [17]. The y-axis represents the air-equivalent distance (range) from the radar. It is possible to distinguish the two components of the signal: the signal of the ground-coupled antennas stands between 0 m and 5 m; the signal of the air-coupled antennas stands between 5 m to 25 m.

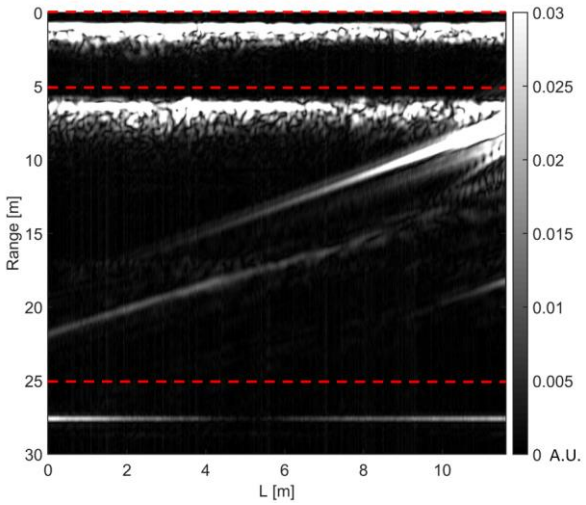


Fig. 17. Example of radargram of the modified GPR.

Since the bands of the two couples of antennas are different, the two contributes can be further separated applying suitable filters. A Butterworth low pass filter of 6 order with 600 MHz cut frequency was applied to data in frequency domain for obtaining the radargram relative to the ground-coupled antennas (Fig. 18). A Butterworth high pass filter of 6 order with 800 MHz cut frequency was applied to data in frequency domain for obtaining the radargram relative to the air-coupled antennas (Fig. 19).

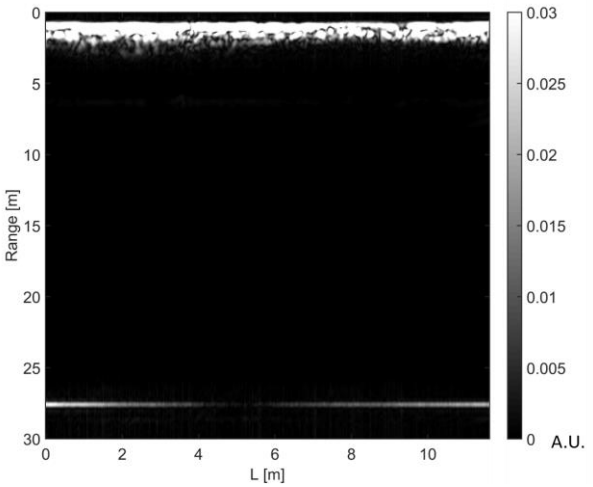


Fig. 18. Radargrams of the ground contribute separated using a Butterworth low pass filter of 6 order with 600 MHz cut frequency

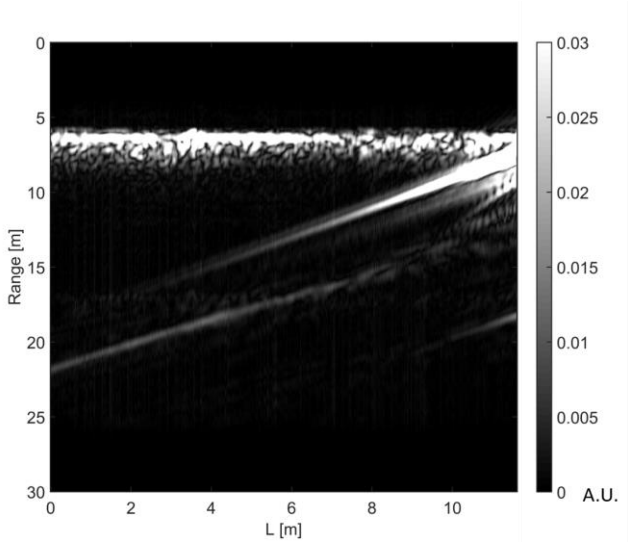


Fig. 19. Radargrams of the air contribute separated using a Butterworth high pass filter of 6 order with 800 MHz cut frequency.

The GPR positions evaluated using (1) have been compared with the odometer data. Fig. 20 shows the comparison between odometer (x-axis) and the position measured by radar (y-axis) during five scans (in different colors). Notice that odometer wheel detects the linear movement of GPR tangent to the ground, while the radar detects the movement along its range. It means that if the ground is not perfectly horizontal the two measurements cannot give exactly the same result.

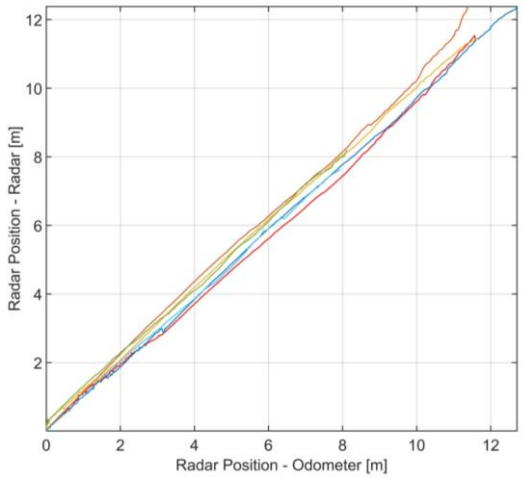


Fig. 20. Comparison between radar and odometer wheel.

The total length measured with radar and with odometer was compared with the length measured with a metric tape. The average ratio between the total length measured using different methods is reported in Table 1. It is possible to note that the total lengths measured using the radar and odometer divided by the value obtained with the tape are both close to 1.

TABLE I
AVERAGE RATIO BETWEEN LENGTH MEASURED WITH DIFFERENT METHOD

| Radar/Tape | Odometer/ Tape | Radar/Odometer |
|---|---|---|
| $0.992 \pm 0.052$ | $1.005 \pm 0.029$ | $0.987 \pm 0.043$ |

The radar has been tested also without odometer in contact with ground (i.e. using the modified odometer rotated by a DC-motor at fixed speed 9.38 rpm). Fig. 21 shows a B-scan obtained using this "auto-positioning" system. The scan length is obtained only using the CR signal as described above.

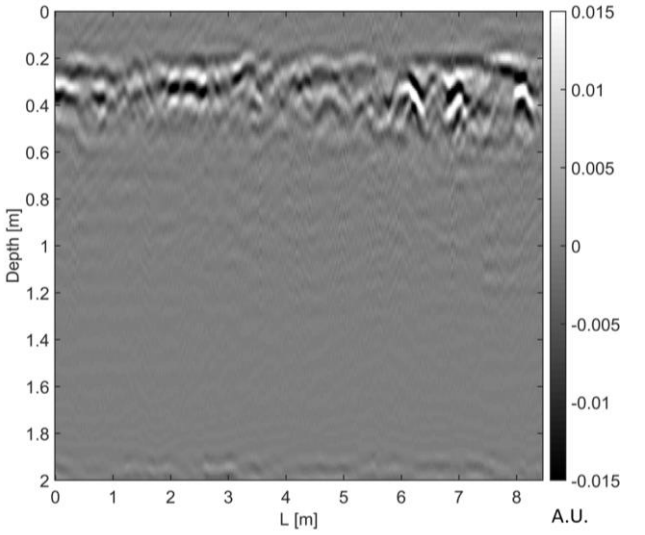


Fig. 21. B-scan using the auto-positioning system.

The performance of this method was evaluated acquiring 9 scans with different lengths and conditions. The average ratio between the distance measured by radar and the distance measured with the tape was $1.008 \pm 0.015$. Therefore, we can state the proposed method can be used as "auto-odometer" for those ground where the wheel-odometers are not suitable.

In some circumstances, the technique described above can be applied even without the use of a CR. This is the case when a wall delimits the scan area. Indeed, the test site shown in the picture in Fig. 16, had a lateral fence wall, that could be used as reference. With the aim to test also this opportunity, some transversal scans (orthogonal to the wall) were performed. Fig. 22 shows the retrieved position using the fence wall as reference. For a single scan of 11.27 m, the standard deviation with respect to odometer data was 85 mm, which is compatible with the accuracy of the odometer itself.

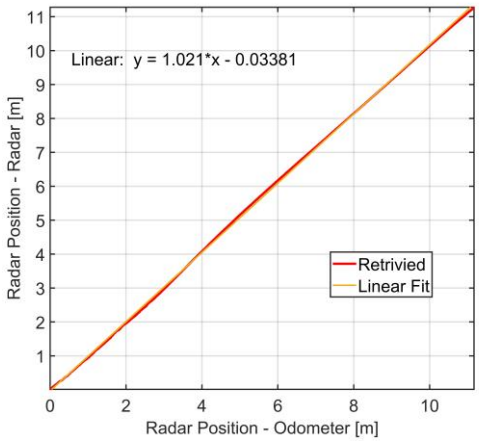


Fig. 22. Comparison between radar and odometer wheel, using a fence wall as reference for the radar

In order to test also the capability of the CR method to retrieve the radar position in two dimensions, a measurement session was performed using two CR. The side of both CR was 1.4 m. As shown in Fig. 23 one of CR was at the center of the coordinates system. The radar movement was approximately along the x-axis (starting from negative values forward CR1). The second corner reflector was located in $(2\ \mathrm{m};\ -3\ \mathrm{m})$.

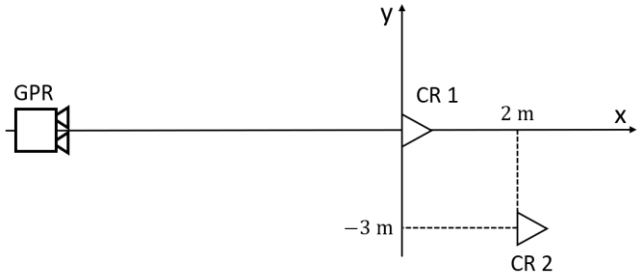


Fig. 23. Measurement geometry for testing the two-dimensional capability of the method

The radargram of the air signal is shown in Fig. 24. The signal of this radargram was saturated in order to emphasize the signal of the two CR. The sliding window was 0.2 m. Fig. 25 shows the retrieved distance of GPR for both CR.

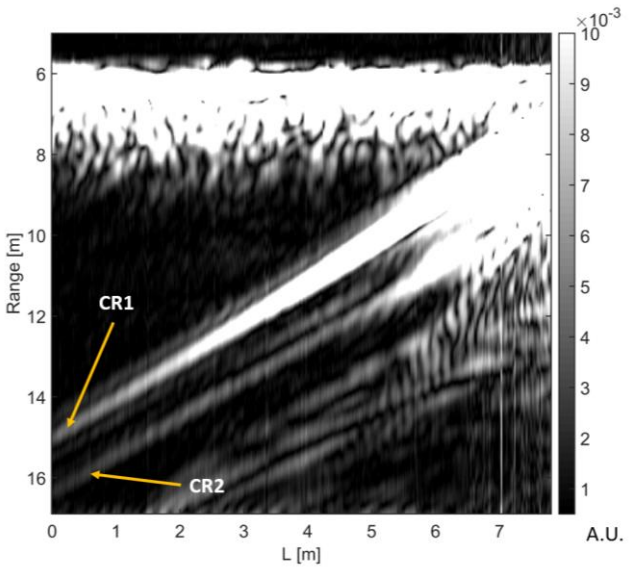


Fig. 24. Radargram of the air signal using two corner reflectors.

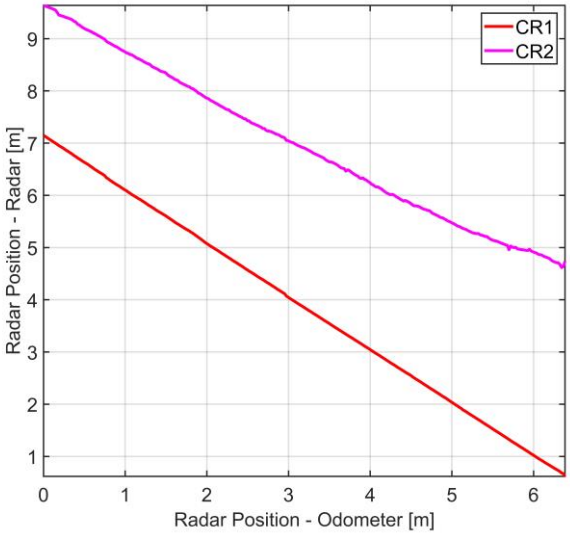


Fig. 25. Retrieved distance of GPR from the two CR.

Finally, the retrieved position of GPR for different measurements was shown in Fig. 26. The initial position of GPR was different for each measurement, but the radar operator tried to follow (pushing by hand) approximately the same straight line.

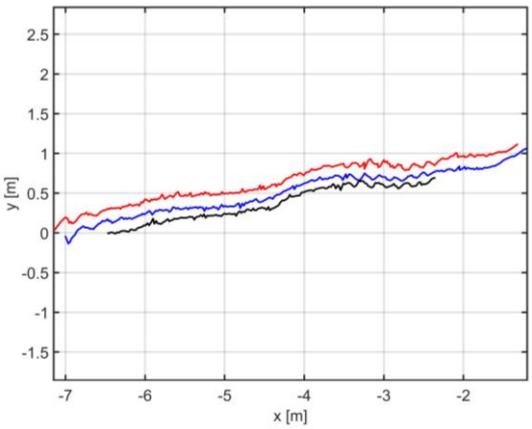


Fig. 26. Retrieved GPR paths.

## V. Discussion

A critical point of the solution proposed in this article is that the radar needs to transmit a large bandwidth signal in air, without a specific license: it can prevent any commercial/industrial implementation of this idea. The radiofrequency spectrum regulation is constantly evolving and, unfortunately, different between countries. The site of European GPR association [18] reports an authoritative collection of the main technical standards in use in Europe, USA and Canada for emissions of GPR equipment. Very basically in Europe the effective radiated power of any unlicensed emission in the band of interest of GPR shall not exceed -37.5 dBm. The effective power radiated in air by the equipment described in this article is about -26 dBm, therefore is technically out of regulation. Nevertheless, an excess of about 10 dB is not so high that it cannot be compensated with suitable design changes. For example, we could use two 28 dB pre-amplifier (instead of only one) in the air receiving chain, by reducing the transmitting power at the regulation limit without sensible loss of Signal-to-Noise Ratio. Furthermore, more radical design changes can dramatically reduce possible interferences with other devices. Currently the radar transmits a sequential ramp of frequencies, but it could easily operate in frequency-hopping spread spectrum (FHSS) modality, that greatly mitigates interferences with other devices operating in the same band [19]. Another possible solution for mitigating possible interferences is to implement a “sniffing and avoiding” strategy [20]: the radar before transmitting a frequency checks that the frequency is not already used. Both CWSF and FHSS radar can tolerate some missing tone without loss of performance.

## VI. Conclusion

An original technique for retrieving the position of a GPR has been proposed and successfully tested. It relies on a hardware upgrade of the antenna subsystem that includes an additional couple of antennas that detect one or two corner reflectors (CR) installed on the ground. In the experimental tests reported in this article the CR are made of solid metal, so they are rather bulky and heavy. Nevertheless, in a practical implementation of this

technique, the CR could be made of wire mesh and designed in light modular pieces.

## REFERENCES


[1] E. Carrick Utsi, *Ground Penetrating Radar: Theory and Practice*, Butterworth-Heinemann, 2017

[2] R. Persico, *Introduction to Ground Penetrating Radar: Inverse Scattering and Data Processing*, IEEE Press Series on Electromagnetism, 2014

[3] M. Grasmueck, D. A. Viggiano, "Integration of ground-penetrating radar and laser position sensors for real-time 3-D data fusion," *IEEE Transactions on Geoscience and Remote Sensing*, vol. 45, no. 1, pp. 130-137, January 2007

[4] G. Manacorda, M. Miniati, A. Sarri, M. Consani, A. Penzo, "Designing a GPR system for the snow-thickness measurement on Mounts Everest and Karakoram," Proceedings of Tenth international conference on Ground penetrating radar. Delft, Netherland 21-24 June 2004

[5] S. Urbini, L. Vittuari, and S. Gandolfi, "GPR and GPS data integration: examples of application in Antarctica," *Annali di Geofisica*, Vol. 44, No. 4, pp. 687-702, August 2001.

[6] F. Dimic, B. Mušič, R. Osredkar, "An example of an integrated GPS and DR positioning system designed for archeological prospecting," *Informacije MIDEM*, vol. 38, no. 2, pp. 144-148, 2008

[7] V. Ferrara, A. Pietrelli, S. Chicarella, L. Pajewski, "GPR/GPS/IMU system as buried objects locator," Measurement, vol. 114, pp. 534-541, 2018

[8] V. Prokhorenko, V. Ivashchuk, S. Korsun, O. Dykovska, "An inertial measurement unit application for a GPR tracking and positioning." In Proceedings of the 12th International Conference on Ground Penetrating Radar (pp. 19-24), 16 Jun 2008 - 19 Jun 2008, Birmingham, UK

[9] S. Li, H. Cai, D. M. Abraham, P. Mao, "Estimating features of underground utilities: Hybrid GPR/GPS approach." *Journal of Computing in Civil Engineering*, Vol. 30, No. 1, Article: 04014108, 2016

[10] R. A. Young, N. Lord, "A hybrid laser-tracking/GPS location method allowing GPR acquisition in rugged terrain." *The Leading Edge*, Vol. 21, No. 5, pp. 486-490, 2002

[11] P. Falorni, L. Capineri, "Optical method for the positioning of measurement points." In 2015 8th International Workshop on Advanced Ground Penetrating Radar (IWAGPR), pp. 1-4, 7-10 July 2015 Florence, Italy

[12] R. Barzaghi, N. E. Cazzaniga, D. Pagliari, L. Pinto, "Vision-based georeferencing of GPR in urban areas." *Sensors*, Vol. 16, No. 1, Article: 132, pp. 1-13, 2016

[13] D. Y. Sukhanov, O. G. Ponomarev, K. V. Zavyalova, V. L. Khmelev, S. N. Roslyakov, Radar with a local positioning video-system. In 2017 Progress In Electromagnetics Research Symposium-Spring (PIERS), pp. 3723-3728, May 2017

[14] F. Parrini, M. Pieraccini, G. Grazzini, A. Spinetti, G. Macaluso, G. De Pasquale, C. Testa, "ORFEUS GPR: a very large bandwidth and high dynamic range CWSF radar." In Proceedings of the XIII International Conference on Ground Penetrating Radar, June 2010

[15] M. Pieraccini, L. Capineri, P. Falorni, D. Devis, "GPR investigation of "Fortezza da Basso"(Lower Fortress) in Florence, Italy." In 2016 16th International Conference on Ground Penetrating Radar (GPR), June 2016.

[16] M. Pieraccini, L. Miccinesi, H. Garcia Canizares, "Critical verification of the underground cartography of the municipality using a high performance Ground Penetrating Radar" 10th International Workshop on Advanced Ground Penetrating Radar, The Hague, The Netherlands, 8-12 September 2019

[17] R. Solimene, A. Cuccaro, A. Dell'Aversano, I. Catapano, F. Soldovieri "Background removal methods in GPR prospecting." In 2013 European Radar Conference, pp. 85-88, Nuremberg, Germany, 9-11 October 2013

[18] http://www.eurogpr.org (viewed on July 2020)

[19] M. J. A. Rahman, M. Krunz, R. Erwin, "Interference mitigation using spectrum sensing and dynamic frequency hopping." In 2012 IEEE International Conference on Communications (ICC), pp. 4421-4425, Ottawa, ON, Canada, 10-15 June 2012

[20] E. Soyak, B, Firat Birlik, M. I.Taskin. "System and method to avoid interference with radar systems." U.S. Patent No. 9,119,079. 25 Aug. 2015.


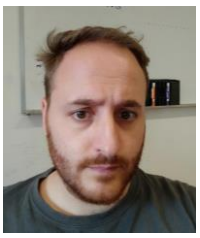

**Lapo Miccinesi** was born in Florence, Italy, in 1988. He received the B.S. degree in physics and M.S. degree in physics of particles from the University of Florence, Florence, in 2011 and 2016, respectively, and Ph.D. degree in information engineering from the University of Florence, Florence, Italy in 2020.

He is currently with the Department of Information Engineering, University of Florence, as a Post-Degree Grant Recipient. His research interests included ground penetrating radar, radar interferometry, ground-based radar, and ground-based synthetic aperture radar.

**Massimiliano Pieraccini** received the M.S. degrees in Physics from the University of Florence, Firenze, Italy, in 1994 and the Ph.D. degree in Non-destructive Testing from University of Florence, Firenze, Italy, in 1998. From 1997 to 2005, he was a Research Assistant with Department of Electronics and Telecommunications (former Department of Electronic Engineering) at the University of Florence, Firenze, Italy. Since 2005, he has been an Associate Professor with the same Department (now Department of Information Engineering).

He is the author of three books, more than 160 articles, and more than 9 patented inventions.

His research interests include ground penetrating radar, ground-based synthetic aperture radar, interferometric radar, microwave sensors